Electronic Supplementary Material (ESI) for Chemical Science.

Supporting information for: Surface Electron Dynamics in Hematite (α-Fe_2O_3): Correlation Between Ultrafast Surface Electron Trapping and Small Polaron Formation

Jakub Husek, Anthony Cirri, Somnath Biswas, and L. Robert Baker*

Department of Chemistry and Biochemistry, The Ohio State University, Columbus, OH 43210

E-mail: baker.2364@osu.edu

Contents

1. Characterization

X-ray Photoelectron Spectroscopy

High resolution XPS analysis was performed on both PC and SC hematite samples under ultrahigh vacuum (1.5 x 10^{-9} Torr) using a Kratos Axis Ultra x-ray photoelectron spectrometer (monochromatic Al Kα X-ray source, $E_{photon} = 1486.6$ eV) to determine oxidation state. The $2p_{3/2}$ transition was fit for all samples using Casa XPS software (Figure S1). All photoelectron spectra were referenced to adventitious carbon at 284.5 eV.

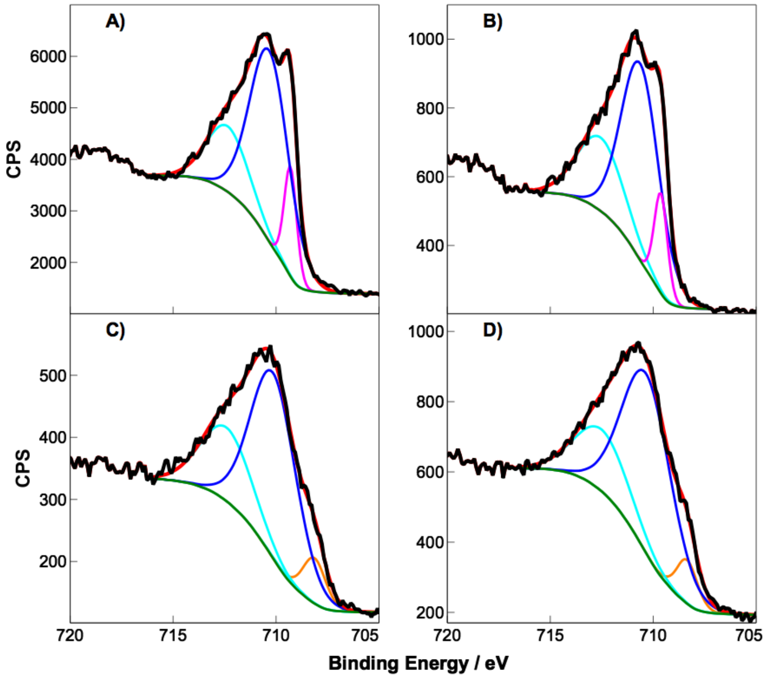

Figure S1: XPS spectra for (A) Fresh SC Fe_2O_3, (B) Fresh PC Fe_2O_3, (C) Used SC Fe_2O_3, and Used PC Fe_2O_3. All measured data is given in black, the colored traces are the individual components used to fit each peak, the red trace is the resulting fit obtained from the sum of the colored traces, and the green baseline is a Shirley background which has been applied to the fit.

From the fits of the fresh SC and PC (B) samples, we assign an oxidation state of 3+ to all iron centers. Both fresh hematite sample fits are in excellent agreement with spectra found in the literature.[S1,S2] However, after the exposure to the 400 nm pump beam, both samples exhibit a small peak centered around 708.25 eV corresponding to Fe^{2+} metal center associated with a slight reduction of the surface. Using the XPS peak fitting, we determine that the Fe^{2+}:Fe^{3+} atomic fraction is ∼6.9% for PC and ∼7.8% for the SC sample, and we find that this has a negligible effect on the observed XUV spectrum such that the role of Fe^{2+} metal centers in this material is neglected in the spectral simulation. The XPS data was collected for the PC sample after a total of 18 s of exposure to the pump beam which resulted in a 7% reduction of the surface. The XPS of the SC sample was taken after 150 s of pump beam exposure, and the surface reduction differed only by 1%. Thus, long term exposure to the pump beam has only negligible effect on the XUV spectrum. All of the XPS fitting parameters are given in Table S1.

Table S1: Fitting parameters for the XPS data presented in Figure S1. The letters in the first column correspond to the ones given in Figure S1, and the peaks are numbered from highest to lowest energy. All positions and widths are in the units of eV.

	Peak 1			Peak 2			Peak 3			Peak 4		
	Position	Width	%	Position	Width	%	Position	Width	%	Position	Width	%
(A)	712.3	2.4	23.7%	710.3	2.2	64.5%	709.3	0.7	11.9%	-	-	-
(B)	712.6	2.7	28.0%	710.6	2.2	61.1%	709.6	0.8	10.8%	-	-	-
(C)	712.4	2.9	28.2%	710.1	2.6	63.6%	709.4	1.0	0.47%	708.1	1.3	7.8
(D)	712.5	3.1	25.6%	710.3	2.8	67.5%	709.2	0.7	0.00%	708.4	1.2	6.9

X-ray Diffraction

Diffraction analysis was performed on the PC Fe_2O_3 by XRD. The X-ray diffraction pattern of PC Fe_2O_3 was collected using a Bruker D8 Discover High-Resolution Triple Axis X-Ray Diffractometer with a Cu Kα source and a scan rate of 10 sec/0.015^o. The diffraction pattern for PC Fe_2O_3 is given below in Figure S2.

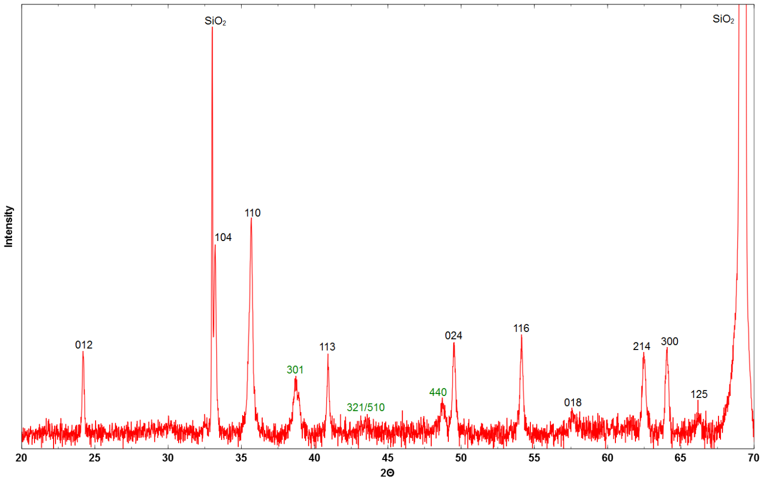

Figure S2: X-ray diffraction pattern for PC Fe_2O_3. Peaks labeled in black correspond to the plane spacing of hematite, while those marked in green belong to the minor impurity phase, β-FeOOH.

2. XUV Probe Spectrum

Figure S3 shows the XUV harmonic spectrum attained upon reflection from SC Fe_2O_3. As described in the main manuscript, a two-color driving field is used to produce both even and odd harmonics. A continuum of XUV photons is produced along the baseline between individual harmonics by slightly chirping the two-color driving field.

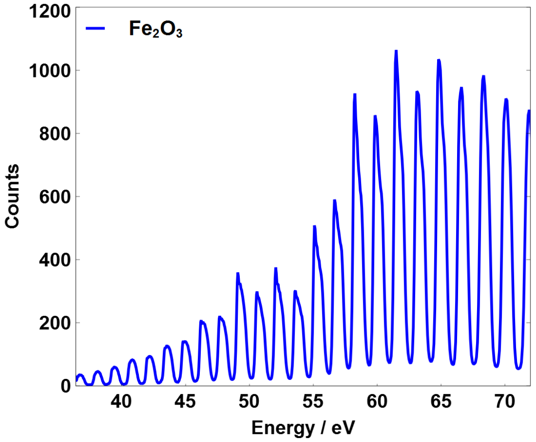

Figure S3: High-harmonic XUV spectrum (36 – 72 eV) collected upon reflection from SC Fe_2O_3.

3. Instrument Response Function

The instrument response function is determined by the convolution of two Gaussians for the bleach kinetics at 54.8 eV for the polycrystalline Fe_2O_3 sample. The fit yields an IRF of 85 ± 30 fs. Figure S4 shows the experimental points (red circles) as well as the fit (blue solid line).

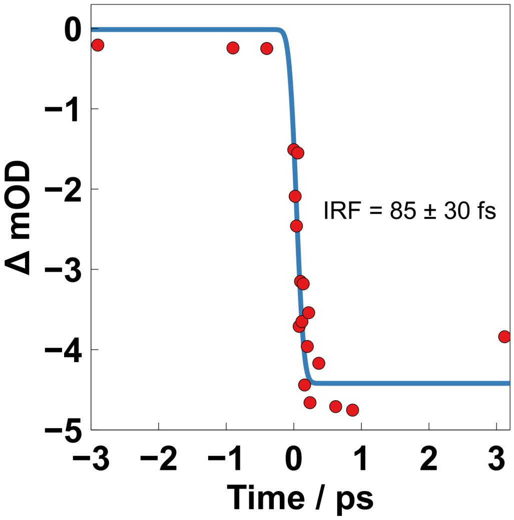

Figure S4: Instrument response function determined from the bleach kinetics at 54.8 eV of the polycrystalline hematite sample.

4. Simulation of Transient Difference Spectra

Table S2: Simulation parameters for obtaining the transmission spectra of Fe^{2+} and Fe^{3+}

	Crystal Field Splitting / eV	Slater Integral Reduction	Fano parameter	Minimum Lorentzian Width / eV	Linear Lorentzian Broadening / eV	Lorentzian Cutoff / eV
Fe^{2+}	1.10	50%	3.5	0.1	0.43	49
Fe^{3+}	1.45	50%	3.5	0.1	0.43	51

Simulations of transient difference spectra presented in the main manuscript were calculated as follows. Since we have previously outlined the full method for simulating XUV-RA ground state spectra in a separate study,[S3] we will only provide a brief description here. The charge transfer multiplet theory code by de Groot and co-workers, CTM4XAS, was used to simulate a "stick" spectrum for Fe^{3+} and Fe^{2+}. Following this, line broadening (Lorentzian, Gaussian, and Fano), and scaling of each spectrum by *d*-orbital occupancy is applied to produce a transmission spectrum in absolute units. All parameters thus far were taken from a previously published work by Leone and co-workers, and the exact values used are given in Table S2.

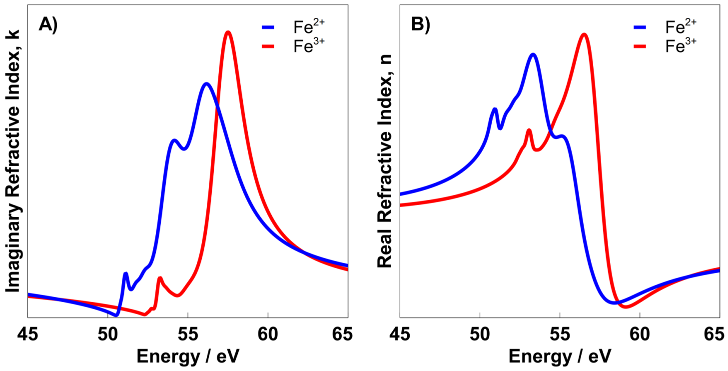

Figure S5: Imaginary (A) and real (B) parts of the refractive index for Fe^{2+} (blue) and Fe^{3+} (red) as derived from the transmission spectra and Kramers-Kronig transformation, respectively. These n and k spectra (with appropriate offset in n for SC or PC) are used to obtain the transient difference spectra.

Following this, k is derived from the transmission spectra and the Kramers-Kronig transformation is then used to derive n for both Fe^{2+} and Fe^{3+}.[S3] The resulting spectra of the real and imaginary parts of the refractive index are shown in Figure S5. Once n and k

are known, the Fresnel coefficient for reflection of *p*-polarized light is used to derive the reflectance spectra. To obtain SC and PC spectra for the Fe^{2+} excited state, all parameters except the oxidation state and the crystal field splitting were fixed based on fits to the corresponding ground state spectra and were not further adjusted during simulation of the transient difference spectra.

5. High Spin Versus Low Spin Transient Excited States

To confirm the high-spin nature of both the initial and final transient states observed experimentally, Figure S6 shows the simulated RA difference spectra (shaded) for high spin Fe^{2+} (A, C, E, and G) and low spin Fe^{2+} (B, D, F, and H) for both the initial (left set of panels) and final (right set of panels) transient excited states. The top panels show results for PC Fe_2O_3, while the bottom panels show the same results for SC Fe_2O_3. The dotted lines are the experimentally measured initial and final state difference spectra, and are shown to assess the quality of the match between the simulated initial and final transient states.

As shown, the initial and final transient difference spectra for the case of high spin and low spin Fe^{2+}, are readily distinguishable, particularly for the case of the final transient state. Because of spin selections rules, the initial Fe^{2+} transient state given by an LMCT photoexcitation is constrained to be high spin. However, given the different spin pairing energies for d^5 Fe^{3+} and d^6 Fe^{2+} metal centers,[S4,S5] formation of the low spin configuration is expected on the ultrafast time scale assuming that there is no reduction in the crystal field splitting (CFS), relative to ground state hematite, upon photoexcitation. Consequently, simulation of the low spin Fe^{2+} is provided here to demonstrate what the final transient spectrum would look like in the absence of lattice expansion as discussed in the main manuscript. As shown, the measured experimental spectrum agrees well with the simulations of the high spin Fe^{2+} metal center for both the initial as well as final transient difference spectra.

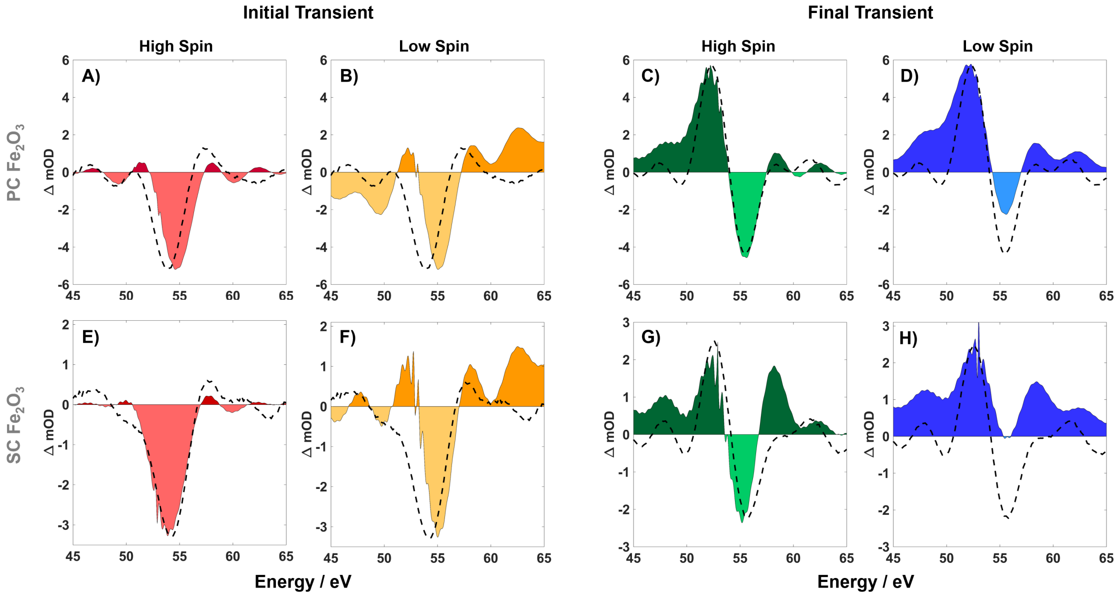

Figure S6: Comparison of experimental transient spectra with simulated difference spectra for high spin and low spin Fe^{2+} excited states. Top panels (A-D) show results for PC Fe_2O_3, and bottom panels (E-H) show analogous results for SC Fe_2O_3. Initial transient spectra are shown on the left for high spin (A and E) and low spin (B and F) Fe^{2+}. Final transient spectra are shown on the right for high spin (C and G) and low spin (D and H) Fe^{2+}. Colored lines show the results of the spectral simulation, and the black dotted line shows the experimentally measured initial and final state spectra. The simulation of high spin Fe^{2+} is more consistent with the experimentally measured spectra for both initial and final transient excited states.

This observation provides additional evidence that lattice expansion around the photoexcited Fe^{2+} – corresponding to small polaron formation – accompanies surface electron trapping. This conclusion is further supported by Figure S7 (analogous to Figure 5 of the main manuscript), where it is apparent that SC Fe_2O_3 follows nearly identical spectral evolution as PC Fe_2O_3, regardless of the different surface morphologies and defect states between these two materials. As discussed in the main manuscript, the observed spectral evolution between initial and final transient states are described by surface electron trapping and a corresponding fast lattice expansion. Surface electron trapping is observed experimentally by the time evolution of the real part of the refractive index, and the corresponding lattice expansion is identified by a 1.5 eV spectral blue shift of the Fe^{2+} excited state. Overall, very good agreement is observed between experiment and theory. However, the final state simulation predicts a positive feature at 58.5 eV that is not observed experimentally. The reason for this singular discrepancy is not yet fully understood and is the subject of ongoing investigation.

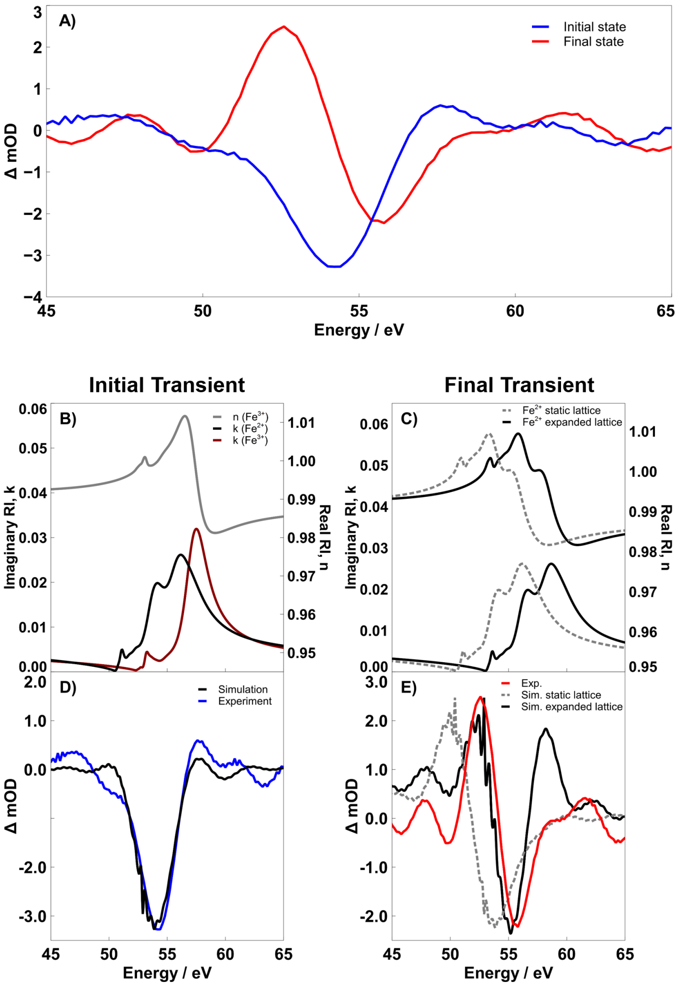

Figure S7: (A) Evolution associated spectra for the initial (blue) and final (red) transient spectra of SC Fe_2O_3 (B,D) The refractive indices used to acquire the initial state simulation are shown in (B). The ground state is described by an $n(\mathrm{Fe}^{3+})$ and $k(\mathrm{Fe}^{3+})$, while the transient state evolves into a transient state described by $n(\mathrm{Fe}^{3+})$ and $k(\mathrm{Fe}^{2+})$. (D) depicts the experimental (blue) and simulated (black) difference spectra. (C,E) The refractive indices used to acquire the final state simulations are shown in (C). In the approximation that lattice expansion does not cause a blue-shift of the spectrum, the transient state is described by the real and imaginary refractive indices for Fe^{2+} shown by the gray-dashed lines. Likewise, a blue-shift associated with lattice expansion leads to the refractive indices given by the black traces. (E) depicts the experimental difference spectrum (red) and simulated difference spectra with (black) and without (gray-dashed) lattice expansion.

6. Influence of Excitation Fraction on RA Difference Spectra

A unique feature to RA spectroscopy is that both n and k are simultaneously measured to give the measured spectrum. However, due to the form of the Fresnel factor, the concentration profile of chemical species sampled within the probe depth of the beam are non-linearly related spectrally, which is in contrast to transmission spectroscopy. To accurately model RA spectra, it is necessary to fractionally weight the linear combination of species within the penetration depth of the probing beam. This indicates that predicting a transient difference spectrum requires a precise knowledge of the excitation fraction. Although this has not been rigorously accounted for in the simulations above, which reflect the difference between pure Fe^{3+} and Fe^{2+} samples, here we consider how excitation fraction will influence the overall shape of the transient difference spectra and demonstrate that this approximation does not adversely affect the state assignments. Figure S8A-D shows the resulting spectra for 1%, 5%, 20%, and 50% contribution of Fe^{2+} to k, respectively, while E-H show the resulting difference spectra for 1%, 5%, 20%, and 50% contribution of Fe^{2+} to both n and k, respectively. For reference, we expect an excitation fraction on the order of 5% based on the pump beam fluence employed here. Based on these simulations we find that qualitatively, the lineshape does not change with excitation fraction and only the change in optical density is affected by considering relative concentrations of the absorbing media. Thus, we have neglected the relative concentrations of Fe^{2+} and Fe^{3+} in the spectra discussed in the main manuscript as this does not affect the conclusions drawn from the state assignments.

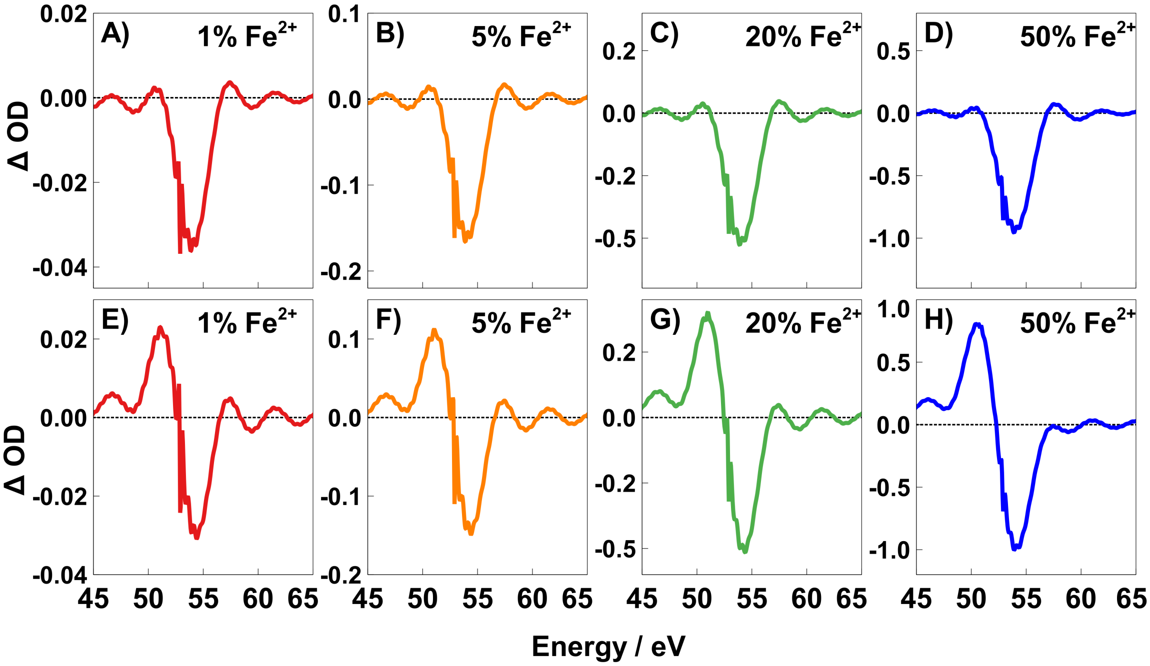

Figure S8: Difference spectra taking into account the non-linearity of the Fresnel factor, using SC Fe_2O_3 as an exemplar. For the upper simulations (A – D), weighted linear combinations of Fe^{3+} and Fe^{2+} define k, where (A) 1%, (B) 5%, (C) 20%, and (D) 50% Fe^{2+} to derive the difference spectrum ($n = Fe^{3+}$). The lower panels (E – H) use weighted linear combinations of Fe^{3+} and Fe^{2+} to define k, and then the Kramers-Kronig relations are used to derive n from this k. The resulting difference spectra shown correspond to (E) 1%, (F) 5%, (G) 20%, and (H) 50% Fe^{2+}.

7. Relative Probe Depth of Real and Imaginary Refractive Index

Since accounting for the relative concentrations of Fe^{2+} and Fe^{3+} does not reproduce the evolution between initial and final transient states, but mixing n and k does, we sought to demonstrate that this is general to the XUV spectral region. To reiterate our findings, we interpret the initial transient state of our ultrafast kinetics as a delocalized state, where the imaginary part of the refractive index has responded to the oxygen-to-iron charge transfer event, while the real part (which responds to the average chemical composition near the surface) exhibits a temporal lag. After 660 fs, the electrons migrate to the surface where the dominant species at the surface is the reduced iron center, and thus n responds to the chemical change. This suggests that there is a difference in penetration depth between n and k, where the latter probes more deeply. As a control, six thin films of TiO_2 on SiO_2 were prepared via atomic layer deposition (growth rate = 0.4 Å / cycle)[S6] and their XUV spectra were recorded (Figure S9A). Our hypothesis for this control is that if k probes more deeply than n, k will respond to *both* TiO_2 and SiO_2 while n will respond to only the surface species, TiO_2. Using a controlled series of thin films with increasing TiO_2 thickness, we would be able to observe how the depth profile affects the measured XUV signal.

Experimentally, we observed that as the thickness of the film increased, the XUV RA spectrum underwent a bathochromic shift in the peak maximum and an increase in RA intensity. To model this, we simulated XUV RA spectra where k is a weighted linear combination of the imaginary refractive indices for TiO_2 and SiO_2, and n corresponds only to TiO_2 (see our previous publication for n and k of TiO_2).[S3] Figure S9B shows the results of these simulations for 20% – 100% contribution of TiO_2 to k. We obtain very good qualitative agreement between theory and experiment, where the former predicts the experimentally observed bathochromic peak shift and increasing RA intensity with increasing TiO_2 film thickness. Based on these results, we draw the conclusion that within our approximation,

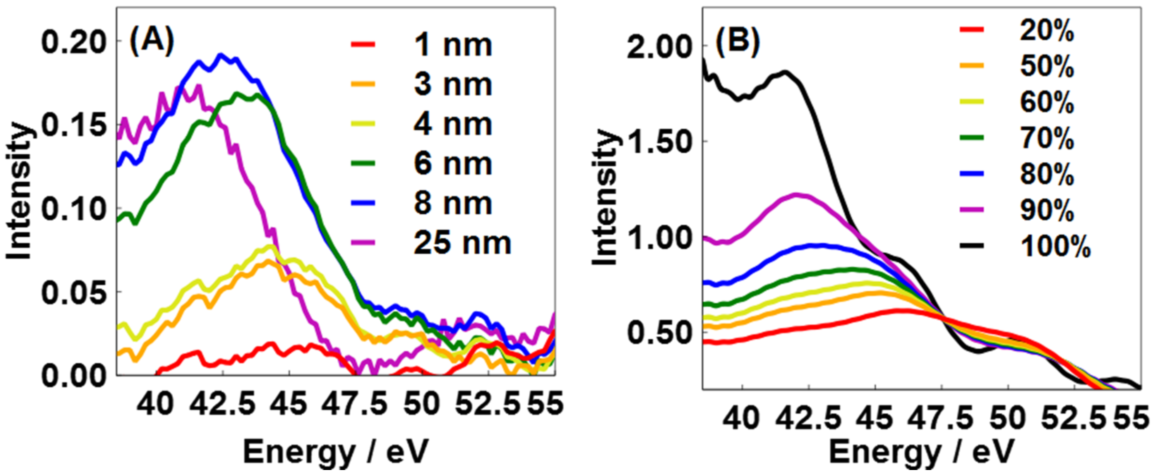

Figure S9: (A) Experimental XUV RA spectra for thin films of TiO_2 between 1 and 25 nm in nominal thickness. (B) Simulations of thin film TiO_2 data, where k is a weighted linear combination of the imaginary refractive indices for TiO_2 and SiO_2 and n corresponds only to TiO_2. The percentages in the key correspond to the fraction of k from TiO_2 used to calculate the simulation.

the probe depth of n is less than that of k – thus indicating that n is more *surface selective* than k. This agrees well with our interpretation of the direction for electron transfer in Fe_2O_3, relative to the surface, that we observe in our kinetic experiment.

References

(S1) Droubay, T.; Chambers, S. A. *Physical Review B* **2001**, *64*, 205414.

(S2) Biesinger, M. C.; Payne, B. P.; Grosvenor, A. P.; Lau, L. W.; Gerson, A. R.; Smart, R. S. C. *Applied Surface Science* **2011**, *257*, 2717–2730.

(S3) Cirri, A.; Husek, J.; Biswas, S.; Baker, L. R. *Submitted* **2017**,

(S4) Griffith, J. S. *J. Inorg. Nucl. Chem.* **1956**, *2*, 1–10.

(S5) Griffith, J. S.; Orgel, L. E. *Q. Rev. Chem. Soc.* **1957**, *11*, 381–393.

(S6) George, S. M. *Chem. Rev.* **2009**, *110*, 111–131.